This manuscript has been published in the journal
Spectrochimica Acta Part A: Molecular and Biomolecular Spectroscopy
https://doi.org/10.1016/j.saa.2025.126990

Spectroscopic investigation of NO transitions near 1915 cm^{-1}: high temperature line parameters and uncertainty quantification

Denghao Zhu [a, *], Sumit Agarwal [b], Bo Shu [b], Ravi Fernandes [b, c], Zhechao Qu [b, *]

a. School of Energy and Environment, Southeast University, Nanjing, China

b. Physikalisch-Technische Bundesanstalt, Braunschweig, Germany

c. Institute of Internal Combustion Engines, Technische Universität Braunschweig, Braunschweig, Germany

∗ Corresponding authors

E-mail addresses: denghao.zhu@seu.edu.cn (D. Zhu); zhechao.qu@ptb.de (Z. Qu)

Abstract

This study presents a comprehensive spectroscopic investigation of two nitric oxide (NO) absorption transitions (Ω1/2 at 1914.99 cm^{-1} and Ω3/2 at 1915.76 cm^{-1}) using laser absorption spectroscopy. By employing two complementary experimental systems, namely a continuous flow gas cell for line intensity measurements and a shock tube facility for temperature dependence coefficient characterization, we attained exceptional measurement accuracy with line intensity uncertainties as low as 0.75% while extending the accessible temperature range to 1742 K. The study systematically characterizes temperature dependence coefficients in four buffer gases (Ar, N_2, He, CO_2), revealing distinct gas-specific behaviours, particularly the weak interaction between NO and helium. A rigorous metrological analysis demonstrated substantial improvements in NO quantification accuracy, achieving 13-fold and 3.5-fold uncertainty reductions for scanned-wavelength and fixed-wavelength LAS, respectively. The development of uncertainty mapping and dynamic uncertainty evaluation methodologies further enhanced measurement reliability under transient conditions. These advancements establish new benchmarks for combustion diagnostics, emissions monitoring, and industrial process control, while providing a transferable framework for precision spectroscopy of other molecular species. The comprehensive dataset and methodological innovations presented in this work address critical gaps in high temperature NO spectroscopy and enable more accurate molecular diagnostics in energy, environmental, and industrial applications.

Keywords: nitric oxide, line intensity, temperature dependency coefficient, uncertainty analysis, laser absorption spectroscopy

1. Introduction

Nitric oxide (NO) plays a pivotal role across diverse scientific and technological domains, ranging from atmospheric chemistry and combustion processes to industrial emissions monitoring. Its accurate quantification is essential for elucidating pollutant formation mechanisms, optimizing combustion efficiency, and ensuring compliance with increasingly stringent environmental regulations [1,2]. However, the detection of NO under practical conditions, particularly at the elevated temperatures and pressures characteristic of combustion systems, presents significant analytical challenges that demand highly precise measurement techniques.

Current NO detection technologies encompass various approaches including chemiluminescence, electrochemical sensors, and spectroscopic techniques [3-5]. Among these, laser absorption spectroscopy (LAS) has emerged as the most competitive solution due to its unique advantages. Unlike chemiluminescence methods that require chemical conversion or electrochemical sensors susceptible to interference, LAS enables quantitative measurement through direct probing of characteristic absorption features at specific wavelengths. This approach offers distinct benefits including non-invasiveness, exceptional molecular selectivity, and rapid temporal response. Notably, LAS achieves high-sensitivity detection at parts-per-billion (ppb) or even parts-per-trillion (ppt) levels while maintaining robust performance in harsh environments with elevated temperatures and pressures, making it particularly suitable for combustion diagnostics and industrial process monitoring applications [6-10].

The accuracy of LAS measurements fundamentally depends on the availability of precise spectroscopic parameters, including line intensities, pressure broadening coefficients, and their temperature dependencies [11-13]. While NO exhibits a strong fundamental absorption band cantered around 5.3 μm, and numerous spectroscopic measurements have contributed to established databases like HITRAN and HITEMP [14-27], several critical gaps remain that limit measurement accuracy. First, many spectroscopic parameters for specific absorption lines are either missing or derived through extrapolation from limited experimental data. Second, most existing parameters were measured using air as the buffer gas, with data for other common buffer gases remaining scarce. Furthermore, most investigations have focused on atmospheric-relevant conditions (<300 K) using Fourier-transform infrared spectroscopy (FTIR), with only limited studies extending to higher temperatures (typically <1000 K) using heated cells. While shock tubes can generate the quasi-instantaneous, homogeneous high-temperature and high-

pressure environments required for more extreme conditions, data on temperature dependence coefficients above 1000 K remain exceptionally scarce.

Building upon our previous work that measured pressure broadening coefficients for two NO absorption peaks (1914.99 cm^{-1} and 1915.76 cm^{-1}, corresponding to R11.5 Ω1/2 and Ω3/2 transitions) [25], the present study addresses remaining uncertainties in NO mole fraction quantification especially for high temperature applications. Our work focuses on determination of line intensities in a static gas cell employing a 140 Hz wavelength-scanned laser system, and acquisition of previously unavailable temperature dependence coefficients across an extended temperature range using a shock tube facility with 20 kHz time-resolution diagnostics. A distinctive feature of this investigation is its comprehensive metrological framework, which incorporates rigorous uncertainty quantification and propagation analysis for both spectroscopic parameters and their impact on practical NO concentration measurements. We systematically evaluate measurement uncertainties associated with both scanned-wavelength and fixed-wavelength LAS strategies. The developed methodology not only provides essential spectroscopic parameters for NO detection in combustion environments but also establishes a robust characterization framework applicable to other molecular species under extreme conditions.

2. Methodology

For LAS, the transmitted intensity $I_t(v)$ of a monochromatic laser source through a gaseous sample is given by Beer-Lambert law [12]:

$$I_t(v) = E(t) + I_0(v) \cdot \eta(t) \cdot exp[-\alpha(v)] \quad (1)$$

with the background emission $E(t)$ at time t, initial laser intensity $I_0(v)$, absorbance $\alpha(v)$, and the broadband transmission losses $\eta(t)$, which are synchronously derived from the individual raw signals and absorption profiles. The exponential term can be computed using the following equation:

$$\alpha(v) = -\ln\left(\frac{I_t(v)-E(t)}{I_0(v)\cdot\eta(t)}\right) \quad (2)$$

The Voigt function can be used to model the line shape of the absorbance spectrum in Eq. (2), which considers the combined effects of Doppler and collisional broadening on the spectral line. These effects are characterized by the Doppler broadening full width at half maximum (FWHM), Δv_D, and the collisional-broadening FWHM, Δv_L, given by

$$\Delta v_D = v_0\sqrt{\frac{8k_B T \ln 2}{Mc^2}} \quad (3)$$

$$\Delta v_L = 2 \cdot p \cdot (\frac{T_0}{T})^n \cdot [\gamma_s \cdot x + \gamma_f \cdot (1 - x)] \quad (4)$$

where k_B is the Boltzmann constant with a value of 1.380649E-23 J/K, T is the temperature, M is the molecular mass of the absorbing species, c is the speed of light, p is the total pressure, x is the mole fraction of NO, γ_s and γ_f are the self and foreign broadening coefficients, T_0 is the reference temperature of 296 K, n is the temperature dependence coefficient. In this study, the contribution of self-broadening is negligible. Therefore, the Equation (4) can be transformed into:

$$\ln\left(\frac{\Delta v_L}{2 \cdot p}\right) = \ln(\gamma_f \cdot (1 - x)) + n \cdot \ln\left(\frac{T_0}{T}\right) \quad (5)$$

The temperature dependence coefficient can be obtained from the slope of the linear regression between $\ln\left(\frac{\Delta v_L}{2 \cdot p}\right)$ and $\ln\left(\frac{T_0}{T}\right)$.

By integrating the absorbance spectrum, the absolute mole fraction can also be obtained by the following equation:

$$A = \int \alpha(v) = \frac{S(T) \cdot p \cdot L \cdot x}{k_B \cdot T} \quad (6)$$

where A is the integrated area of the absorbance, L is the optical path length. Then, the line intensity can be obtained using following equation:

$$S(T) = m \cdot \frac{k_B \cdot T}{L \cdot x} \quad (7)$$

where m is the slope of the linear fit between absorbance area and pressure.

3. Experimental setup

To measure the line intensity and temperature dependence coefficient, two in-house LAS-based spectrometers have been developed. Figure 1(a) and Figure 1(b) represent the setup for line intensity and temperature dependence coefficient measurement, respectively. The details of these two setups will be introduced below.

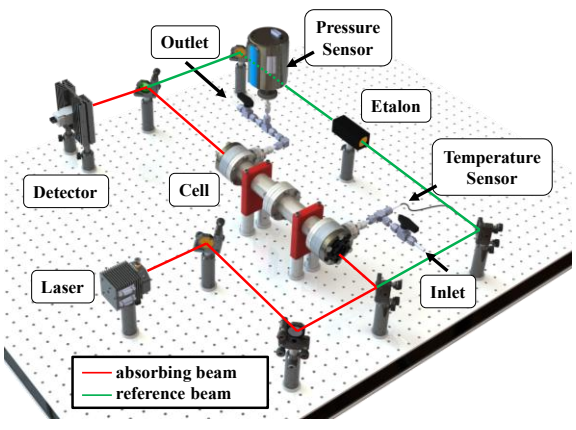

(a) line intensity

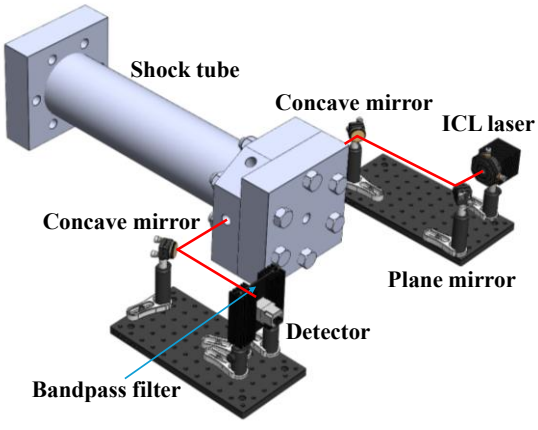

(b) temperature dependence coefficient

Figure 1. Schematic of the experimental setup

The line intensity measurements were performed in a continuous-flow stainless steel gas cell (optical path length: 35.52 cm) equipped with wedged CaF_2 windows to minimize etalon effects. A certified reference gas mixture (Linde, 2001 ppm NO in N_2, ±0.5% uncertainty) was used for absolute NO concentration calibration. The NO laser is a continuous-wave distributed-feedback interband cascade laser (CW-DFB-ICL, Nanoplus) with a tunable wavenumber ranging from 1913-1920 cm^{-1}. The laser wavelength was tuned by a laser diode controller (PRO8000 equipped with LDC8002 and TED8020, Thorlabs) together with a function generator (KEYSIGHT, 33500B). The tuning frequency was set as 70 Hz with a triangle-shaped current ramp. A detector (PVI-4TE-5, VIGO) was used to receive the laser signal focused by a concave mirror. To ensure accurate wavelength calibration, a reference beam was directed through a Germanium etalon (76.244 mm length, Physikalisch-Technische Bundesanstalt (PTB)-traceable) to monitor the laser tuning. The etalon transmission peaks enabled precise conversion of the temporal signal into wavenumber space. High-fidelity signal acquisition was achieved using a 16-bit resolution data acquisition system (USB-6363, National Instruments) sampling at 600 kHz. Pressure was monitored using a calibrated capacitance manometer (MKS Baratron, 0–100 mbar range), while temperature was measured using a PT100 thermocouple (traceable to PTB standards). Both sensors were calibrated against SI-traceable references from PTB.

For temperature-dependent coefficient measurements, we employed a shock tube facility consisting of a 3.5-meter driver section and 4.5-meter driven section (7 cm inner diameter) to generate well-controlled, transient high temperature and pressure conditions [11]. The system was instrumented with five Kistler 603CAB pressure sensors and an MKS Baratron for initial pressure measurement (P_1), while post-shock conditions (P_2, T_2, P_5, T_5) were determined via one-dimensional shock wave relations. Figure 1(b) shows the coupling of shock tube and LAS setup in both two-dimension and three-dimension views. To accommodate the microsecond-scale phenomena, we significantly enhanced our laser absorption spectroscopy capabilities by increasing the scan frequency to 20 kHz. The laser beam passed through optical windows positioned in the same plane as the fourth pressure sensor and focused onto a photodetector (PVI-4TE-5, VIGO). To minimize background interference, such as thermal emission from shock-heated gases, a narrow bandpass filter (center wavelength: 5219 nm, bandwidth: 30 nm, Laser Components) was positioned in front of the detector. Both the pressure and photodetector signals were captured using a 16-bit data acquisition card (M2p.5943-x4, Spectrum Instrumentation) operating at a sampling rate of 80 MS/s.

4. Results and discussions

4.1 Line intensity

Nitric oxide (NO) possesses a ground electronic state characterized as a $^2\Pi_\Omega$ state due to its unpaired electron configuration, where the subscript Ω represents the absolute value of the combined spin and orbital electronic angular momentum projection along the molecular axis. This electronic structure gives rise to distinct rotational-vibrational transitions, with the fundamental vibrational band exhibiting two closely spaced sub-bands. Each sub-band contains *R* and *P* branches, along with a weak *Q* branch, where the line numbering follows $m=-J$ for the *P* branch and $m=J+1$ for the *R* branch (*J* being the rotational quantum number). Building upon our previous spectroscopic investigations [25], the current work focuses on refining the line parameters for two specific NO absorption features in the 5.2 μm fundamental band, as illustrated in Figure 2. Spectral analysis reveals that the first absorption feature (Peak 1, Ω1/2) at 1914.99 cm^{-1} consists of two sub-peaks centered at 1914.985 cm^{-1} and 1914.993 cm^{-1}, each comprising five transition lines. Similarly, the second feature (Peak 2, Ω3/2) at 1915.76 cm^{-1} contains ten transition lines in total. Both absorption peaks correspond to *R*-branch transitions with identical line numbers ($m=11.5$).

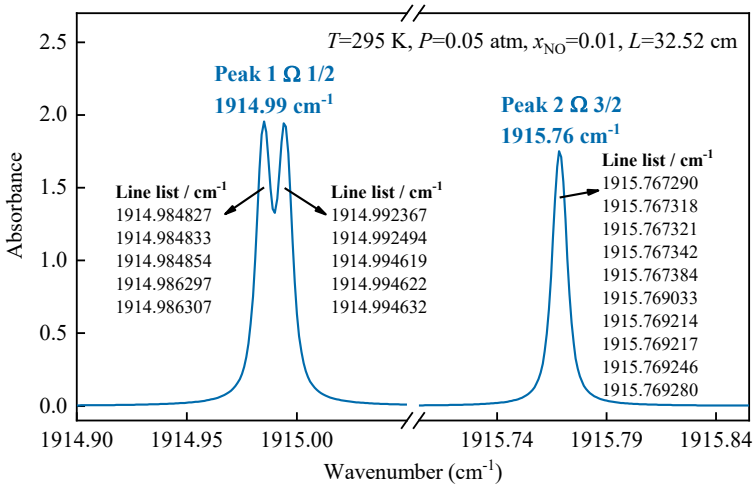

Figure 2. Simulated NO absorption peaks investigated in this study based on HITRAN database

In the present experimental configuration, the spectral resolution is insufficient to resolve individual transitions within each absorption peak due to their close proximity. However, all ten transitions comprising each peak exhibit identical spectroscopic parameters, such as pressure broadening coefficients and temperature dependence characteristics. This equivalence allows us to model the entire absorption feature using a multi-line Voigt profile fitting approach, where all transitions within a peak are treated collectively. The reported line intensities and temperature dependence coefficients are thus assigned to each composite absorption peak as a

whole, maintaining consistency with our previous methodology for pressure broadening coefficient determinations [25].

Accurate line intensity measurements necessitate precise knowledge of the NO concentration. Given the strong absorption cross-sections of these transitions, the use of pure NO would lead to complete signal saturation. To circumvent this limitation, we employed a certified reference gas mixture containing 2001 ppm NO in N_2 (Linde, ±0.5% uncertainty). The experimental system used continuous gas flow to minimize potential adsorption effects. For enhanced spectral characterization, the two absorption peaks were measured independently. As shown in Figure 3, the raw absorption signals and corresponding etalon reference data (for 1915.76 cm^{-1}) were acquired. Wavenumber calibration was achieved through third-order polynomial fitting of the etalon peaks, yielding a free spectral range (FSR) of 0.0163 cm^{-1} at the measurement wavelength of 5.22 μm (refractive index = 4.0145). This calibration procedure ensures precise spectral axis determination for subsequent lineshape analysis.

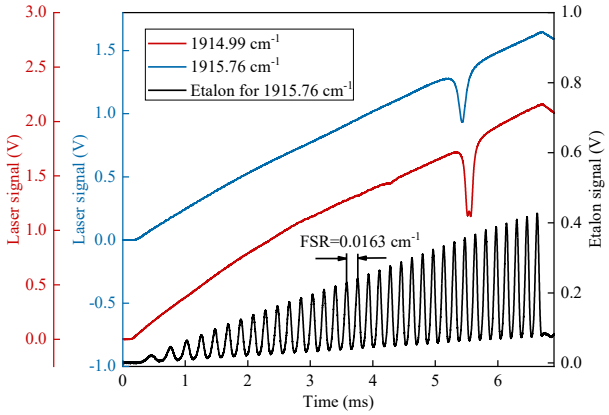

Figure 3. Raw data of laser signal and etalon signal measured in the gas cell

Following the Beer-Lambert law, the acquired laser transmission signals were converted to absorbance spectra as presented in Figure 4(a). The absorbance profiles were subsequently analyzed using Voigt profile fitting based on Equations (3-4), showing good agreement with the experimental data as evidenced by residual standard deviations below 0.002. While Equation (7) theoretically permits line intensity determination from a single pressure measurement, we conducted a pressure-dependent study to minimize systematic uncertainties. The selection of lower pressure conditions enabled clear separation of the two subpeaks comprising Peak 1, thereby enhancing fitting accuracy. Figure 4(b) displays the linear pressure dependence of integrated absorbance areas for both absorption peaks, where error bars incorporate ±1% pressure measurement uncertainty (coverage factor k=1) on the x-axis, and combined standard deviations of absorbance areas and wavenumber calibration uncertainties

(1%) on the y-axis [12,13]. Linear regression analysis yielded slopes of 0.14109±0.00147 and 0.07205±0.00057 for Peak 1 and Peak 2 respectively, with residuals consistently below 0.0001.

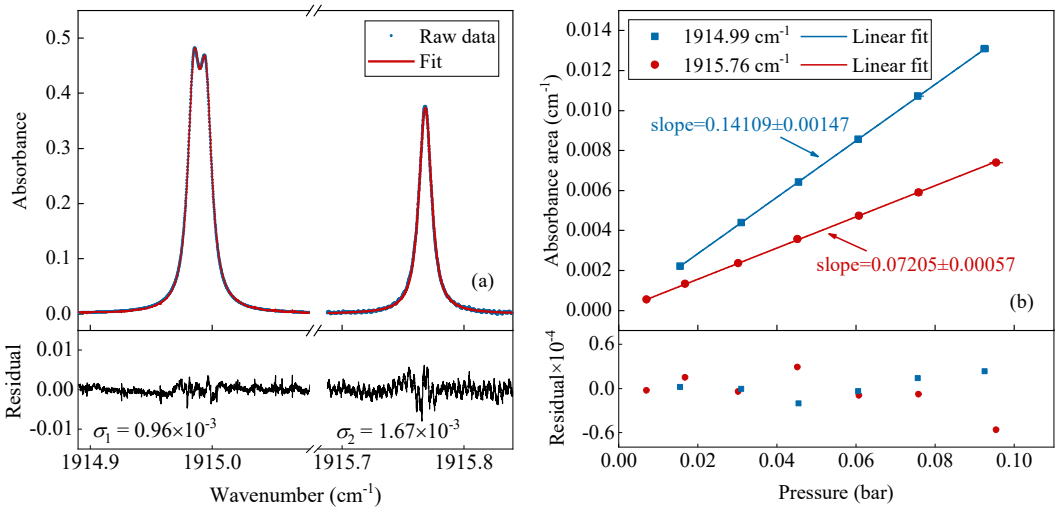

Figure 4. (a) NO absorption spectra; (b) Absorbance area at different pressure of two peaks (the x and y axis error bars are hidden within the symbol)

Historical context for these measurements is provided in Figure 5 and Table 1, which compile previously reported line intensities spanning five decades of spectroscopic research. Early measurements by Abels and Shaw (1966) employed grating spectrometers [14], while subsequent studies by Mandin et al. (1980) [15], Ballard et al. (1988) [18], and Spencer et al. (1994) [19] utilized FTIR spectroscopy. The most recent quantum cascade laser (QCL)-based measurements by Almodovar (2019) achieved improved precision through advanced laser technology [22]. In the latest version of HITRAN 2020 database, the line intensities of these two peaks were adopted from the calculation results by Coudert et al. in 1995 [21]. From the comparison results in Table 1, post-1980 results exhibit remarkable consistency (<10% variation), reflecting technological advancements in spectroscopic instrumentation. For uncertainty quantification, we applied the metrological framework outlined in the 'Guide to the Expression of Uncertainty in Measurement' (GUM). The combined standard uncertainty $u(x)$ is derived as the positive square root of the total variance [28]:

$$u(x) = \sqrt{\sum_{i=1}^{N} \left(\frac{\partial f}{\partial Y_i} \cdot u(Y_i)\right)^2} \tag{8}$$

where $u(Y_i)$ is the uncertainty of the i_{th} quantity Y_i

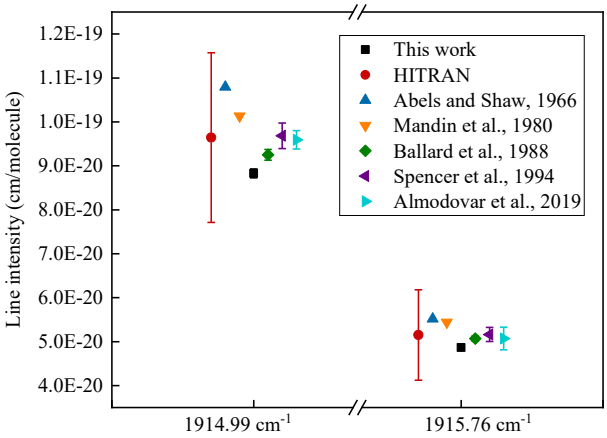

Figure 5. Comparison of line intensity with literature results

Table 1. The sum of line intensities for Peak 1 and Peak 2

	Peak 1 Ω1/2 (1914.99 cm^{-1})	**Peak 2 Ω3/2 (1915.76 cm^{-1})**
1966, Abels and Shaw [14]	1.0792E-19	5.5185E-20
1980, Mandin et al. [15]	1.0130E-19	5.4400E-20
1988, Ballard et al. [18]	9.2500E-20 (1.3%)	5.0700E-20 (1.18%)
1994, Spencer et al. [19]	9.6815E-20 (3%)	5.1613E-20 (3.12%)
2019, Almodovar et al [22]	9.5919E-20 (2.2%)	5.0710E-20 (5.1%)
HITRAN [26]	9.6421E-20 (20%)	5.1506E-20 (20%)
This study	**8.8279E-20 (1.15%)**	**4.8643E-20 (0.75%)**

Table 1 demonstrates that our measurements achieve exceptional measurement precision, with relative uncertainties of just 1.15% and 0.75% for Peak 1 (Ω1/2) and Peak 2 (Ω3/2) respectively. To elucidate the sources of uncertainty, a comprehensive breakdown for the Ω3/2 transition is performed in Table 2. The uncertainty budget shows that the dominant contributions arise from the linear regression slope (m) of the pressure-dependent absorbance measurements and the certified NO mole fraction (x) in the reference gas. The slope uncertainty primarily reflects the precision of spectral fitting procedure and absorbance area integration, while the mole fraction uncertainty originates from the reference gas certification process. Overall, the absolute uncertainties of all quantities are small. The high precision achieved in this work stems mainly from high-resolution wavelength-scanned laser spectroscopy, rigorous statistical treatment of pressure-dependent measurements and use of traceable reference materials with certified uncertainties.

Table 2. Uncertainty of line intensity for Peak 2 Ω3/2 (1915.76 cm^{-1})

Quantity	k_B	L	x	m	T
Value	1.380649E-23 J/K	32.52 cm	0.0002001	0.07773	294.95 K

Uncertainty (%)	-	0.1	0.5	0.55	0.0063
Contribution (%)	-	1.8	44.4	53.7	0.1
Line intensity	**4.8643E-20 ± 3.648E-22 (0.75%)**				

4.2 Temperature dependence coefficients

For high temperature applications such as combustion systems and thermal industrial processes, the temperature dependence coefficient of spectroscopic parameters becomes critically important for accurate mole fraction determination. To establish well-characterized high-temperature conditions, we employed a shock tube facility capable of generating three distinct thermodynamic states: pre-shock condition (P_1, T_1), post-incident shock condition (P_2, T_2), and post-reflected shock condition (P_5, T_5). Figure 6 presents representative time-resolved measurements of both laser absorption signals and pressure profiles for a 1% NO/99% Ar mixture, with pressure data acquired from the fourth transducer along the shock tube.

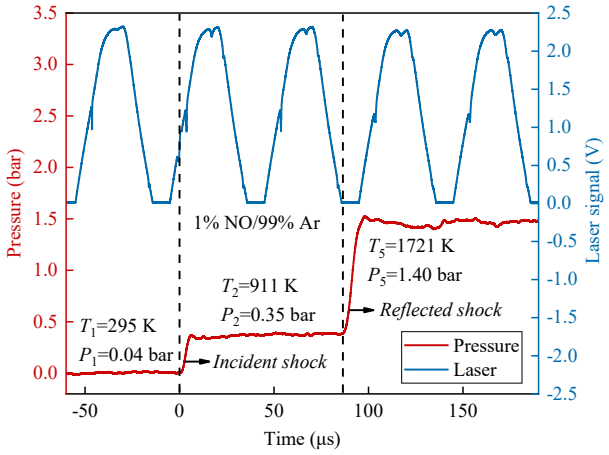

Figure 6. Dynamic laser signal and pressure measured in the shock tube (1915.76 cm^{-1})

In a typical experiment, the driven section was initially filled with test gas at 0.04 bar. Following diaphragm rupture, the incident shock wave produced near instantaneous (within 7 μs) increases to 911 K and 0.35 bar. Subsequent reflection of the shock wave at the endwall further elevated conditions to 1721 K and 1.4 bar within 10 μs. Our measurement strategy represents a significant advancement over conventional shock tube spectroscopy, incorporating ultra-high-speed laser scanning at 20 kHz to capture spectroscopic data during both the incident and reflected shock phases. This innovation not only doubles the effective data yield from each experiment but also substantially extends the accessible temperature range from 595 K (P_2, T_2) to 1742 K (P_5, T_5), which is a 400 K improvement over traditional reflected-shock-only measurements. The expanded temperature coverage proves particularly valuable for

characterizing the temperature dependence of spectroscopic parameters across thermally relevant ranges encountered in practical applications.

Figure 7(a) presents a detailed view of the transmitted laser signals during a half-period scan, where the baseline was characterized using a third-order polynomial fit. The corresponding absorbance spectra across all three shock wave stages are displayed in Figure 7(b), indicating distinct temperature and pressure effects on the spectral line profiles. As the system transitions from the initial conditions (P_1, T_1) to reflected shock conditions (P_5, T_5), several key spectroscopic phenomena become evident. The overall spectral width increases noticeably due to pressure broadening. Meanwhile, the line intensity displays a non-monotonic dependence on temperature, reaching a maximum absorption strength near 450 K. Additionally, subtle shifts in the peak center positions occur as a result of combined thermal and pressure effects. These observations provide direct experimental evidence of the complex interplay between thermodynamic conditions and NO absorption characteristics, with the high temporal resolution (20 kHz) enabling clear separation of the distinct shock tube phases.

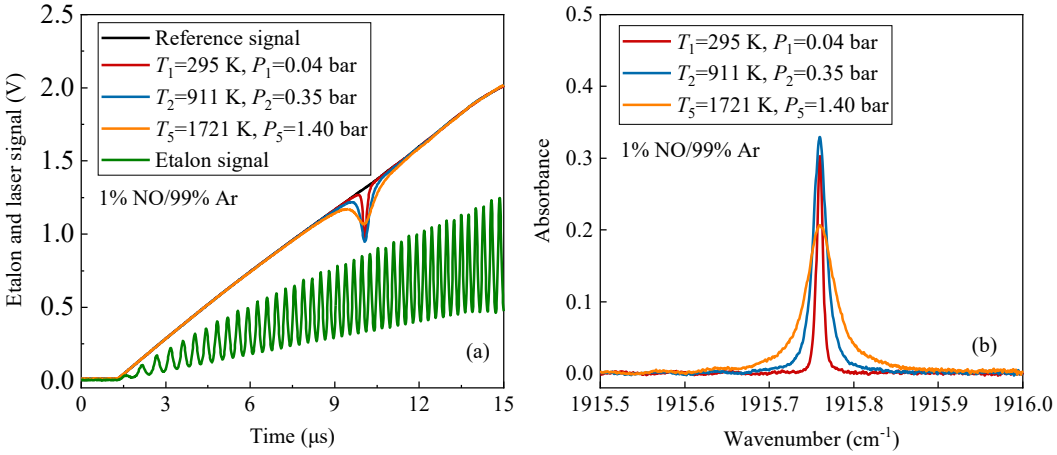

Figure 7. (a) Etalon signal and laser signal; (b) Absorbance of NO at different status measured in the shock tube (1915.76 cm^{-1})

The absorbance profiles measured at both post-shock conditions (P_2, T_2) and post-reflected shock conditions (P_5, T_5) were analyzed using Voigt profile fitting with a nonlinear Levenberg-Marquardt optimization algorithm, as demonstrated in Figure 8. The fitting quality was good for both thermodynamic states, yielding residuals of 2.3×10^{-3} and 3.0×10^{-3} optical density (1σ standard deviation) respectively.

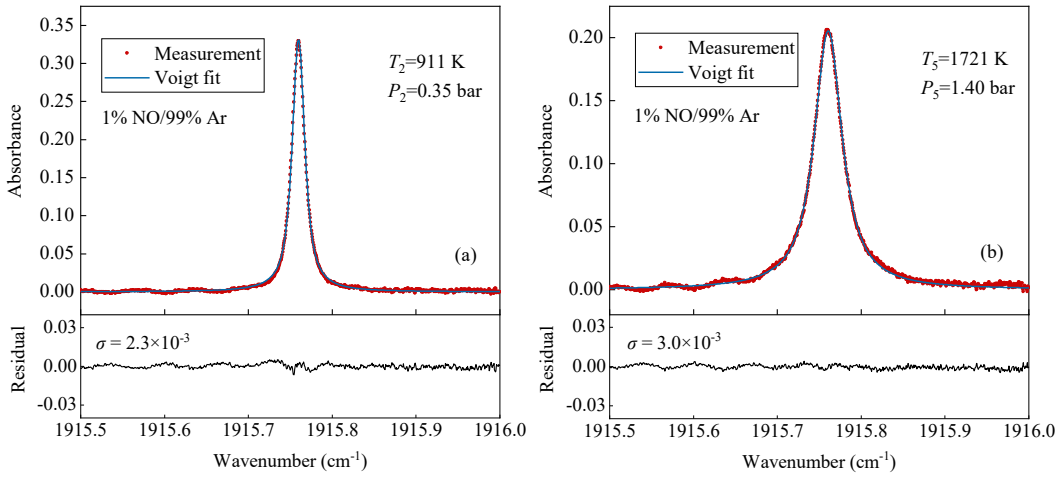

Figure 8. NO absorption spectra and Voigt fit for 1% NO/99% Ar mixture (1915.76 cm^{-1})

Figure 9 presents the complete dataset of pressure-normalized line widths plotted against temperature. The error bars account for measurement uncertainties in temperature (1.35% for T_2 and 1.8% for T_5) and pressure (2% for P_2 and 2.8% for P_5) determinations, with all uncertainties reported at k=1 based on our previous systematic investigations [29]. Following Equation (5), the temperature dependence coefficients were derived from the slope of linear regressions between the natural logarithm of normalized line widths ($\ln\left(\frac{\Delta\nu_L}{2\cdot p}\right)$) and the inverse temperature ratio ($\ln\left(\frac{T_0}{T}\right)$), where this logarithmic transformation effectively linearizes the temperature-power law relationship while properly accounting for the experimental uncertainties in both coordinates.

The temperature dependence coefficients for both Peak 1 (Ω1/2, 1914.99 cm^{-1}) and Peak 2 (Ω3/2, 1915.76 cm^{-1}) were systematically characterized in four buffer gases: Ar, N_2, He, and CO_2. As shown in Figure 9, the temperature sensitivity varies among different collision partners. In particular, NO–He mixtures exhibit weaker temperature dependence compared to the other buffer gases. This observation is consistent with our previous findings for carbon monoxide (CO) and highlights fundamental differences in intermolecular interactions. The reduced temperature sensitivity in helium can be attributed to its unique physical properties—it is a light, monatomic, and chemically inert gas that interacts with NO primarily through weak van der Waals forces. In contrast, heavier noble gases (Ar), diatomic molecules (N_2), and polar species (CO_2) produce stronger collisional effects, resulting in more pronounced temperature-dependent behavior. These differences arise from enhanced dipole interactions, greater momentum transfer during collisions, and stronger attractive forces in the intermolecular potential. The consistent trends observed in both NO and CO systems suggest that such

temperature dependence characteristics may represent a general feature of collisional broadening and shifting in light molecular absorbers.

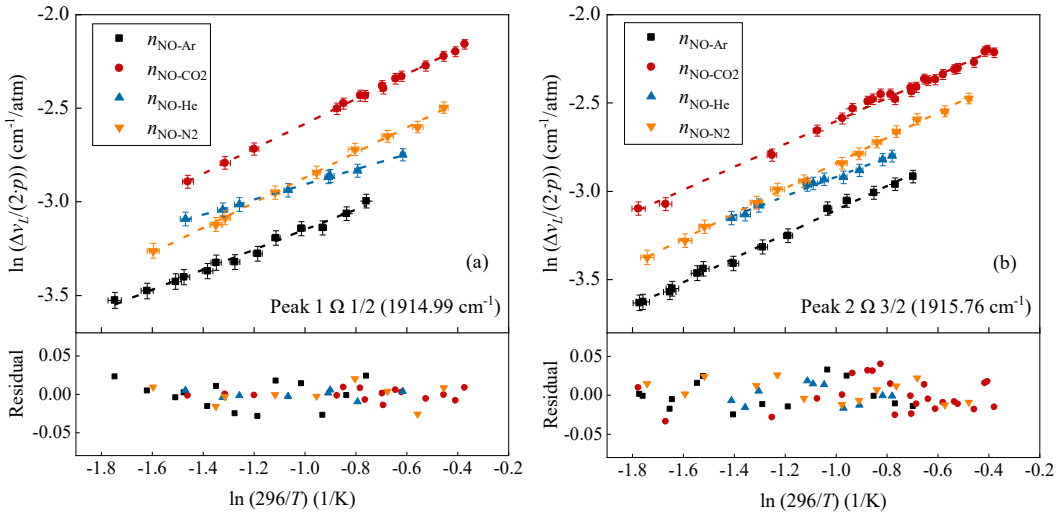

Figure 9. Temperature dependence coefficients of NO measured in this study

Figure 10 and Table 2 present a comprehensive comparison of our measured temperature dependence coefficients with existing literature data, where values in parentheses indicate measurement uncertainties. Historical measurements reveal a notable evolution in the spectroscopic characterization of NO collisions. In 1998, Ballard and Johnston conducted a pioneering FTIR study of NO–N_2 collisions over the temperature range of 213–296 K [18]. A decade later, Spencer et al. performed similar FTIR measurements spanning 183–296 K, obtaining consistent results for the Ω1/2 transition, but reporting divergent values for the Ω3/2 line [20]. A significant advancement occurred in 2019, when Almodovar et al. utilized tunable diode laser absorption spectroscopy (TDLAS) to investigate NO–N_2 and NO–Ar systems at temperatures up to 802 K using a heated gas cell [22].

Our current work extends this progress by providing the first high-temperature data (>800 K) for NO-N_2 and NO-Ar systems and reporting the inaugural measurements of NO-CO_2 and NO-He temperature dependencies for both transitions. Our results show close agreement with Almodovar's data, especially when compared to earlier FTIR studies. This likely stems from the overlapping temperature ranges in our experimental conditions (595–1742 K vs. 294–802 K) and the precision advantages of modern TDLAS over traditional FTIR methods. This consistency across independent TDLAS studies conducted with different experimental configurations reinforces the reliability of our measurements and highlighting the technological advancements in spectroscopic instrumentation over the past three decades. The newly acquired data for CO_2 and He buffer gases fill critical knowledge gaps in high temperature NO

spectroscopy, enabling more accurate molecular diagnostics in combustion systems where these species are prevalent.

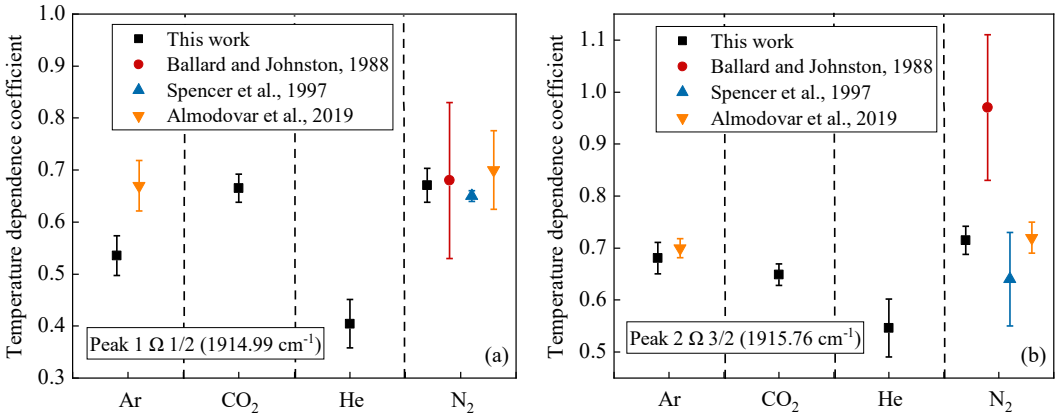

Figure 10. Comparison of temperature dependency coefficients with literature results

Table 2. Summary of NO temperature dependency coefficients

Year and authors	Technique	Temp. (K)	Peak 1 Ω1/2 (1914.99 cm^{-1})				Peak 2 Ω3/2 (1915.76 cm^{-1})			
			Ar	CO_2	He	N_2	Ar	CO_2	He	N_2
1988, Ballard and Johnston [18]	FTIR	183~296				0.68 (15)				0.97 (14)
1997, Spencer et al. [20]	FTIR	183~296				0.65 (10)				0.64 (90)
2019, Almodovar et al. [22]	TDLAS/ Gas cell	294~802	0.67 (48)			0.7 (76)	0.7 (18)			0.72 (30)
2025, this study	**TDLAS/ Shock Tube**	**430-1750**	**0.536 (38)**	**0.665 (27)**	**0.404 (47)**	**0.671 (33)**	**0.681 (30)**	**0.649 (20)**	**0.546 (56)**	**0.715 (27)**

The uncertainties are given in parentheses.

4.3 Uncertainty analysis of NO mole fraction

The reliability of spectroscopic measurements depends on both absolute accuracy and rigorous uncertainty quantification. The current study has characterized line intensities and temperature dependence coefficients for the Ω1/2 (1914.99 cm^{-1}) and Ω3/2 (1915.76 cm^{-1}) transitions. Combined with our previous determinations of pressure broadening coefficients, these results now provide complete spectroscopic characterization of these absorption features. To assess the practical impact of these improved parameters, detailed uncertainty analysis for prevalent scanned-wavelength and fixed-wavelength LAS are conducted. This evaluation demonstrates how refined spectroscopic data enhances NO quantification accuracy in real-world applications.

4.3.1 Scanned-wavelength LAS

The discussion begins with an uncertainty analysis of scanned-wavelength LAS, which depends solely on line intensity and is independent of other spectral line parameters based on Equation (6). As a case study, we utilize NO mole fraction measurements obtained from a flow

reactor in our previous work [30], where the concentration was determined using the absorption peak of the Ω3/2 transition at 1915.76 cm^{-1}. Figure 11 presents the temperature-dependent NO concentration profile (700-1150 K) with corresponding uncertainty bounds. While the absolute difference between our measured line intensity and HITRAN database values is modest (<6%), the impact on measurement uncertainty proves dramatic, achieving a 13-fold reduction in total uncertainty. This significant improvement arises from a fundamental restructuring of the uncertainty budget, as demonstrated in Table 3. Notably, the relative contribution of line intensity uncertainty decreases dramatically from 99.4% to just 21.9% of the total uncertainty. This analysis demonstrates that for scanned-wavelength LAS, even minor improvements in line intensity accuracy can yield disproportionate benefits for overall measurement precision.

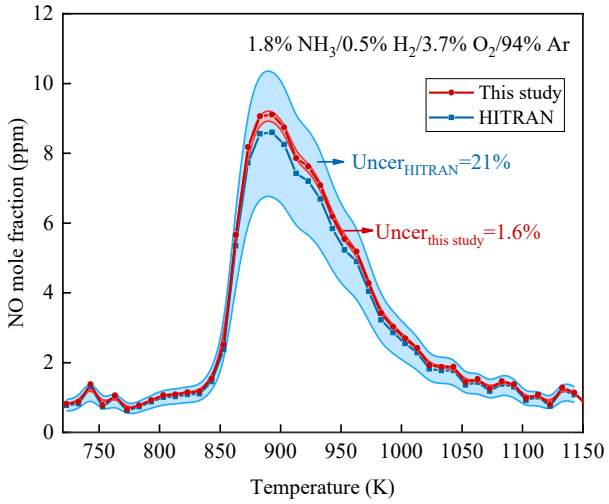

Figure 11. Temperature-resolved NO mole fraction of $NH_3/H_2/O_2$/Ar mixture measured in a flow reactor [30] using the line intensity from HITRAN and this work

Table 3. Uncertainty budgets of NO mole fraction using line intensity from HITRAN and this work for scanned-wavelength method

Quantity	This Study			HITRAN		
	Value	**Uncer. (%)**	**Contr. (%)**	**Value**	**Uncer. (%)**	**Contr. (%)**
k_B	1.380649E-23 J/K	–	–	1.380649E-23 J/K	–	–
L	3122.7 cm^{-1}	0.064	0.2	3122.7 cm^{-1}	0.064	0.1
A	0.0067	1	38.9	0.0067	1	0.2
S	4.8643E-20 cm/mol	0.75	21.9	5.1506E-20 cm/mol	20	99.4
T	300 K	0.0062	0.1	300 K	0.0062	0.1
P	0.2 bar	1	38.9	0.2 bar	1	0.2
x_{NO}	**9.13 ppm**	**1.6**		**8.6 ppm**	**21**	

4.3.2 Fixed-wavelength LAS

For combustion diagnostics requiring high temporal resolution, fixed-wavelength LAS is the preferred measurement approach. In this configuration, NO mole fraction determination

involves solving the coupled nonlinear Equations (1-4). In contrast to scanned-wavelength methods, fixed-wavelength LAS introduces additional complexity by incorporating pressure broadening, temperature dependence and gas matrix into the uncertainty analysis. The measurement uncertainty propagation follows a multivariate relationship where the mole fraction (x_{NO}) exhibits complex correlations with multiple quantities as:

$$x_{NO} = f(\alpha(v), L, p, T, v_0, S, \gamma_i, n_i, x_i) \quad (9)$$

The terms γ_i and n_i represent the pressure broadening coefficient and the temperature dependence coefficient, respectively, for the interaction between NO and the *i*th component in the gas mixture. x_i denotes the mole fraction of the *i*th component in the mixture, which are involved in the calculation of Lorentzian line width.

While our previous study conducted uncertainty analysis for the fixed-wavelength method [31], it did not account for uncertainties arising from variations in the gas matrix composition. The current investigation advances the uncertainty evaluation methodology by incorporating the uncertainties associated with gas component mole fractions. As a case study, the time-resolved NO profiles from previous shock tube study of NH_3 oxidation (4% NH_3/6% O_2/90% Ar) are usd [31], where measurements were performed at 0.5 μs resolution with the laser centred at 1915.76 cm^{-1} characterized by a wavemeter (671B, Bristol Instruments). The comparative uncertainty analysis in Table 4 indicates that while NO concentrations derived from our parameters and HITRAN data agree within 10%, our measurements achieve a 3.5-fold reduction in total uncertainty from 30.78% to 8.89%. This improvement primarily stems from three critical advancements: the replacement of estimated air-broadening coefficients with direct Ar-broadening measurements ($\gamma_{NO\text{-}Ar}$), the implementation of experimentally determined temperature exponents ($n_{NO\text{-}Ar}$), and the use of refined line intensity values. Note that except for 90% argon in the mixture, the remaining 10% gas components are dynamically changing during oxidation that is difficult to calculate precisely. For simplicity, those 10% rest components are taken as a whole. We adopted $\gamma_{NO\text{-}Air}$ values with 20% uncertainty and assign $n_{NO\text{-}rest}$ with a default value of 0.5 [13]. The analysis confirms that line intensity uncertainty remains the dominant factor, though its contribution decreases substantially when using our measured parameters. This case study highlights how comprehensive spectroscopic characterization enables more accurate fixed-wavelength LAS in reactive flows, despite the inherent challenges of transient composition changes and competing uncertainty sources in high-speed combustion diagnostics.

Table 4. Uncertainty budgets of NO mole fraction using line parameters from HITRAN and our measurement for fixed-wavelength method

Quantity	Our measurement			HITRAN		
	Value	**Uncer. (%)**	**Contr. (%)**	**Value**	**Uncer. (%)**	**Contr. (%)**
$\alpha(v)$	0.12	4.2	22.33	0.12	4.2	1.87
L	7 cm	1.1	1.53	7 cm	1.1	0.13
p	4 bar	1.5	0.038	4 bar	1.5	0.004
T	2500 K	2.2	12.71	2500 K	2.2	1.001
v_0	1915.76 cm^{-1}	0.0001	8.85E-12	1915.76 cm^{-1}	0.0001	4.25E-13
$S(T_0)$	4.8643E-20 cm/molecule	0.75	0.71	5.1506E-20 cm/molecule	20	42.34
$\gamma_{NO\text{-}Ar}$	0.04264 cm^{-1}/atm	0.52	11.52	0.0561 cm^{-1}/atm	10	0.67
$\gamma_{NO\text{-}rest}$	0.058 cm^{-1}/atm	20	0.18	0.058 cm^{-1}/atm	20	5.96
$n_{NO\text{-}Ar}$	0.6805	4.4	12.86	0.68	20	0.76
$n_{NO\text{-}rest}$	0.5	20	25.92	0.5	20	46.42
x_{Ar}	0.9	1%	0.68	0.9	1%	0.059
x_{rest}	0.1	20%	11.51	0.1	20%	0.78
$\boldsymbol{x_{NO}}$	**0.009**	**8.89**		**0.01**	**30.78**	

The investigation extends to dynamic measurement conditions encompassing wide pressure and temperature ranges. Figure 12(a) presents a comprehensive uncertainty map for NO mole fraction determination across 1600-2800 K and 2-6 bar. The analysis demonstrates that measurement uncertainty increases systematically with temperature while showing an inverse relationship with pressure. Temperature variations exert a more pronounced influence than pressure changes due to their dominant role in the uncertainty budget, as evidenced in Table 4. This behaviour originates from temperature's dual impact on both spectroscopic parameters through the temperature dependence coefficient n and on Boltzmann population distributions.

The practical application of this analysis is illustrated in Figure 12(b), which showcases shock tube measurements at T_5=1880 K and P_5=3.4 bar. The time-resolved NO profile integrates dynamic uncertainty quantification derived from the mapping in Figure 12(a). Temperature values are calculated using our PTB/NH_3-C_2 mechanism [32] with pressure inputs from high-speed transducer measurements.

While absolute uncertainty variations across experimental conditions remain within a relatively narrow band, this methodology represents a significant advancement for precision dynamic measurements. This novel approach enables real-time uncertainty quantification in transient environments while providing temperature-compensated concentration readings. It accounts for the coupled thermodynamic effects on spectral parameters, which are particularly challenging in shock tube kinetics studies where traditional uncertainty estimation methods often fail to capture these dynamic interactions. The framework supports mechanism validation through uncertainty-aware species profiles and establishes new standards for traceability in extreme condition measurements.

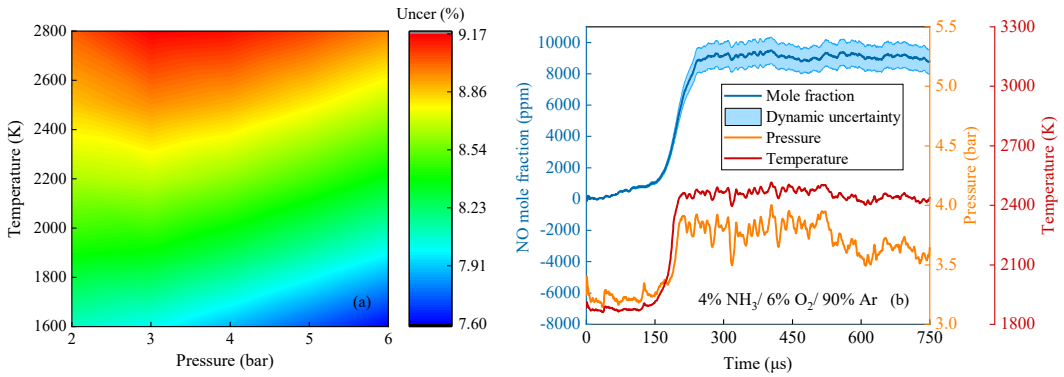

Figure 12. (a) Uncertainty map of NO mole fraction; (b) Time-resolved NO mole fraction of $NH_3/O_2/Ar$ mixture measured in a shock tube with dynamic uncertainty inferred from uncertainty map

The above uncertainty analysis demonstrates that precise spectroscopic parameters are fundamental to achieving minimal uncertainty in mole fraction quantification. This conclusion carries significant implications across the entire spectrum of gas sensing applications, where enhanced measurement accuracy directly translates to improved reliability in concentration determination. In environmental monitoring systems, such precision advancements enable more robust detection of atmospheric pollutants at lower concentration thresholds, while in industrial settings they facilitate tighter process control through more accurate real-time gas composition analysis. The capability to discern finer concentration variations proves particularly transformative for combustion diagnostics, where subtle changes in NOx levels often serve as critical indicators of combustion efficiency and pollutant formation mechanisms.

5. Conclusions

This study systematically measured the line intensities and temperature dependence coefficients of two NO absorption peaks (Peak 1 Ω1/2 at 1914.99 cm^{-1} and Peak 2 Ω3/2 at 1915.76 cm^{-1}) using laser absorption spectroscopy (LAS). To ensure measurement accuracy over a wide temperature range, two distinct experimental setups were utilized: a continuous-flow gas cell for line intensity measurements and a shock tube for determining the temperature dependence coefficients at high temperature.

High precision line intensity measurements were achieved using a certified reference gas, with uncertainties as low as 1.15% and 0.75% for the two peaks, respectively. Results align closely with modern literature but exhibit significantly lower uncertainties. Novel shock tube methodology enabled measurements in four buffer gases (Ar, N_2, He, CO_2), capturing the absorption spectrum not only after reflected shock wave but also after incident shock wave within 100 μs (T_2, P_2), extending the temperature range beyond prior studies. The shock tube

measurements reveal distinct gas-dependent behaviors, particularly the weak interaction between NO and helium with a lower temperature dependence compared to other buffer gases (Ar, N_2, CO_2), consistent with theoretical predictions.

Metrological uncertainty analysis has been performed for both scanned-wavelength and fixed-wavelength LAS. For scanned-wavelength LAS, using our measured line parameters reduced NO mole fraction uncertainty by 13-fold, primarily by diminishing the dominant contribution of line intensity uncertainty (from 99.4% to 21.9%). For fixed-wavelength LAS, uncertainty decreased by 3.5 times (from 30.78% to 8.89%). The development of uncertainty mapping and dynamic uncertainty evaluation methodologies further enhanced measurement reliability under transient conditions.

These advancements directly support more stringent emissions compliance monitoring, improved early detection capabilities for gas leakage systems, and definitive interpretation of kinetic data in combustion and atmospheric chemistry research. The methodology developed herein provides a transferable framework for precision spectroscopy of other molecular species, promising broad impacts across analytical chemistry, process control, and environmental monitoring applications.

Declaration of interests

None

Credit authorship contribution statement

Denghao Zhu: Investigation, Visualization, Writing – original draft; **Sumit Agarwal**: Investigation, Writing – review and editing; **Bo Shu**: Writing – review and editing; **Ravi Fernandes**: Writing – review and editing; **Zhechao Qu**: Investigation, Writing – review and editing.

Acknowledgement

The project (23IND09 MaritimeMET) has received funding from the European Partnership on Metrology, co-financed by the European Union's Horizon Europe Research and Innovation Programme and by the Participating States. Denghao Zhu thank the support from "the Fundamental Research Funds for the Central Universities" (No.4003002506).

References

[1] J.A. Logan, Nitrogen oxides in the troposphere: Global and regional budgets, J. Geophys. Res.: Oceans, 88 (2012) 10785-10807.

[2] L.D.S. S.C. Hill, Modeling of nitrogen oxides formation and destruction in combustion systems, Prog. Energy Combust. Sci., 26 (2000) 417–458.

[3] E.M. Hetrick, M.H. Schoenfisch, Analytical chemistry of nitric oxide, Annu Rev Anal Chem (Palo Alto Calif), 2 (2009) 409-433.

[4] Matthews, Ronald D. and Sawyer, Robert F. and Schefer, Robert W., Interferences in chemiluminescent measurement of nitric oxide and nitrogen dioxide emissions from combustion systems, Environ. Sci. Technol., 11 (1977) 1092-1096.

[5] M.D. Brown, M.H. Schoenfisch, Electrochemical Nitric Oxide Sensors: Principles of Design and Characterization, Chem Rev, 119 (2019) 11551-11575.

[6] R.K. Hanson, D.F. Davidson, Recent advances in laser absorption and shock tube methods for studies of combustion chemistry, Prog. Energy Combust. Sci., 44 (2014) 103-114.

[7] A. Farooq, A.B.S. Alquaity, M. Raza, E.F. Nasir, S. Yao, W. Ren, Laser sensors for energy systems and process industries: Perspectives and directions, Prog. Energy Combust. Sci., 91 (2022) 100997.

[8] S. Barrass, Y. Gerard, R.J. Holdsworth, P.A. Martin, Near-infrared tunable diode laser spectrometer for the remote sensing of vehicle emissions, Spectrochim Acta A Mol Biomol Spectrosc, 60 (2004) 3353-3360.

[9] K. Duan, D. Wen, Y. Ji, K. Xu, Z. Huang, X. Zhang, S. Yao, W. Ren, Quantum cascade laser absorption sensor for in-situ, real-time and sensitive measurement of high-temperature SO_2 and SO_3, Spectrochim Acta A Mol Biomol Spectrosc, 309 (2024) 123864.

[10] Y. Li, Y. Ma, C. Zheng, D. Yu, L. Hu, S. Yang, F. Song, Y. Li, S. Liu, Z. Zhang, Y. Zhang, Y. Wang, F.K. Tittel, Near-infrared wide-range dual-gas sensor system for simultaneous detection of methane and carbon monoxide in coal mine environment, Spectrochim Acta A Mol Biomol Spectrosc, 307 (2024) 123581.

[11] D. Zhu, S. Agarwal, L. Seifert, B. Shu, R. Fernandes, Z. Qu, NH_3 absorption line study and application near 1084.6 cm^{-1}, Infrared Phys. Technol., 136 (2024) 105058.

[12] D. Zhu, L. Seifert, S. Agarwal, B. Shu, R. Fernandes, Z. Qu, NH_3 line broadening coefficients and intensities measurement and impurities determination in emerging applications: CCUS, Biomethane and H_2, Spectrochim Acta A Mol Biomol Spectrosc, 320 (2024) 124642.

[13] D. Zhu, L. Seifert, S. Agarwal, B. Shu, R. Fernandes, Z. Qu, Measurement of carbon monoxide pressure broadening and temperature dependence coefficients in the 1←0 band, Phys. Chem. Chem. Phys., 27 (2025) 7004-7015.

[14] L.L. Abels and J.H. Shaw, Widths and Strengths of Vibration-Rotation lines in the Fundamental Band of Nitric Oxide, J. Mol. Spectrosc., 20 (1966) 11-28.

[15] J. Y. Mandin, C. Amiot, G. Guelachvili, Intensity and self-broadening coefficient measurements from Fourier transform spectra: application to the nitric oxide fundamental band, Annales de Physique, 5 (1980) 91-111.

[16] P.K. Falcone, R.K. Hanson, C.H. Kruger, Tunable diode laser measurements of the band strength and collision halfwidths of nitric oxide, J. Quant. Spectrosc. Radiat. Transf., 29 (1983) 205-221.

[17] J.P. Houdeau, C. Boulet, J. Bonamy, A. Khayar, G. Guelachvili, Air broadened NO linewidths in a temperature range of atmospheric interest, J. Chem. Phys., 79 (1983) 1634-1640.

[18] J. Ballard, W.B. Johnston, B.J. Kerridge, J.J. Remedios, Experimental Spectral Line Parameters in the 1-0 Band of Nitric Oxide, J. Mol. Spectrosc., 127 (1988) 70-82.

[19] M.N. Spencer, C. Chackerian, L.P. Giver, L.R. Brown, The Nitric Oxide Fundamental Band: Frequency and Shape Parameters for Rovibrational Lines, J. Mol. Spectrosc., 165 (1994) 506-524.

[20] M.N. Spencer, C. Chackerian, L.P. Giver, L.R. Brown, Temperature Dependence of Nitrogen Broadening of the NO Fundamental Vibrational Band, J. Mol. Spectrosc., 181 (1997) 307-315.

[21] L.H. Coudert, V. Dana, J. Y. Mandin, M. Morillonchapey, R. Farrenq, G. Guelachvili, The spectrum of nitric oxide between 1700 and 2100 cm^{-1}, J. Mol. Spectrosc., 172 (1995) 435-448.

[22] C.A. Almodovar, W.W. Su, C.L. Strand, R.K. Hanson, R-branch line intensities and temperature-dependent line broadening and shift coefficients of the nitric oxide fundamental rovibrational band, J. Quant. Spectrosc. Radiat. Transf., 239 (2019).

[23] R.J. Hargreaves, I.E. Gordon, L.S. Rothman, S.A. Tashkun, V.I. Perevalov, A.A. Lukashevskaya, S.N. Yurchenko, J. Tennyson, H.S.P. Müller, Spectroscopic line parameters of NO, NO_2, and N_2O for the HITEMP database, J. Quant. Spectrosc. Radiat. Transf., 232 (2019) 35-53.

[24] S. Yang, W. Peng, B. Yu, X. Sun, S. Zhou, J. Li, Measurement of nitric oxide spectral parameters: Considering the effects of CO_2 and H_2O, Spectrochim Acta A Mol Biomol Spectrosc., 283 (2022) 121749.

[25] S. Agarwal, L. Seifert, D. Zhu, B. Shu, R. Fernandes, Z. Qu, Investigations on Pressure Broadening Coefficients of NO Lines in the 1←0 Band for N_2, CO_2, Ar, H_2, O_2 and He, Appl. Sciences, 13 (2023) 13031370.

[26] I. E. Gordon, L. S. Rothman, R. J. Hargreaves, R. Hashemi, E. V. Karlovets, F. M. Skinner, E. K. Conway, C. Hill, R. V. Kochanov and Y. Tan, et al., The HITRAN2020 molecular spectroscopic database, J. Quant. Spectrosc. Radiat. Transf. 277 (2022) 107949.

[27] L.S. Rothman, I.E. Gordon, R.J. Barber, H. Dothe, R.R. Gamache, A. Goldman, V.I. Perevalov, S.A. Tashkun, J. Tennyson, HITEMP, the high-temperature molecular spectroscopic database, J. Quant. Spectrosc. Radiat. Transf., 111 (2010) 2139-2150.

[28] International Organization for Standardization (ISO), ISO Guide 98-3, Guide to the Expression of Uncertainty in Measurement; International Organization for Standardization: Geneva, Switzerland, 2008; ISBN 9267101889.

[29] D. Zhu, S. Agarwal, B. Shu, R. Fernandes, Z. Qu, An ultra-rapid optical gas standard for dynamic processes: Absolute NH_3 quantification and uncertainty evaluation, Measurement, 230 (2024) 114559.

[30] D. Zhu, L. Ruwe, S. Schmitt, B. Shu, K. Kohse-Hoinghaus, A. Lucassen, Interactions in Ammonia and Hydrogen Oxidation Examined in a Flow Reactor and a Shock Tube, J Phys Chem A, 127 (2023) 2351-2366.

[31] D. Zhu, Z. Qu, M. Li, S. Agarwal, R. Fernandes, B. Shu, Investigation on the NO formation of ammonia oxidation in a shock tube applying tunable diode laser absorption spectroscopy, Combust. Flame., 246 (2022) 112389.

[32] M. Li, D. Zhu, H. Karas, S. Agarwal, Z. Qu, K. Moshammer, R. Fernandes, B. Shu, NH_3/C_2H_6 and NH_3/C_2H_5OH oxidation in a shock tube: Multi-speciation measurement, uncertainty analysis, and kinetic modeling, Chem. Eng. J., 498 (2024) 155041.